Anomalous Lattice Softening Near a Quantum Critical Point in a Transverse Ising Magnet

Keisuke Matsuura,[1,*] Pham Thanh Cong,[2] Sergei Zherlitsyn,[2] Joachim Wosnitza,[2,3]
Nobuyuki Abe,[1] and Taka-hisa Arima[1]

[1]*Department of Advanced Materials Science, the University of Tokyo, Kashiwa 277-8561, Japan*
[2]*Dresden High Magnetic Field Laboratory (HLD-EMFL) and Würzburg-Dresden Cluster of Excellence ct.qmat, Helmholtz-Zentrum Dresden-Rossendorf, 01328 Dresden, Germany*
[3]*Institut für Festkörper- und Materialphysik, Technische Universität Dresden, 01062 Dresden, Germany*

(Received 1 October 2019; revised manuscript received 16 January 2020; accepted 28 February 2020; published 26 March 2020)

We have investigated the elastic response of a transverse Ising magnet $CoNb_2O_6$ by means of ultrasound velocity measurement. A huge elastic anomaly in the C_{66} mode is observed near a quantum critical point when sweeping a magnetic field perpendicular to the Ising axis. This anomaly appears to become critical only for the Faraday configuration (field parallel to the sound propagation direction) but is much less pronounced for the Voigt geometry (field perpendicular to the sound propagation direction). We propose that the relativistic spin-orbit interaction plays a crucial role in the quantum critical regime resulting in the elastic anomaly, which is enhanced by quantum fluctuations.

DOI: 10.1103/PhysRevLett.124.127205

Quantum critical behavior is a central issue in condensed matter physics. Various remarkable phenomena, such as exotic superconductivity and non-Fermi liquid behavior, appear around the quantum critical points (QCPs), which are induced by purely quantum mechanical interactions [1–5]. The long-range order is broken by quantum fluctuations at a critical value of a tuning parameter such as magnetic field, pressure, or doping [6]. A prototypical system which undergoes a quantum phase transition is an Ising spin chain in a transverse magnetic field, called the transverse Ising model. It was recently reported that $CoNb_2O_6$ behaves as a transverse Ising magnet (TIM) when a magnetic field is applied along the magnetic hard axis [7]. To date, a variety of studies about TIM have been performed [6–10]. It is relatively easy to access the QCP in $CoNb_2O_6$ experimentally because of the moderate critical magnetic field of 5.4 T. Most of the previous studies on $CoNb_2O_6$ were, however, focused on investigating the magnetic excitations near the QCP by using inelastic neutron scattering (INS) [7], terahertz spectroscopy [11], and nuclear magnetic resonance [12]. In a macroscopic study, Liang *et al.* revealed that the heat capacity was largely enhanced at the QCP [13]. For further exploring macroscopic properties in this unique system, we focus on the orbital state of Co^{2+} ions in the ground state. The strong Ising anisotropy is caused by the spin-orbit interaction (SOI) which means that the Co^{2+} ions are in a spin-orbit entangled state [14], as seen in $KCoF_3$ [15], $GeCo_2O_4$ [16], etc. Here, we study how spin-orbit-coupled fluctuations and the elastic properties are involved in the quantum critical regime near the QCP.

$CoNb_2O_6$ belongs to the columbite family with the orthorhombic space group *Pbcn* [Fig. 1(a)]. The lattice constants are $a = 14.170$ Å, $b = 5.715$ Å, and $c = 5.048$ Å. Co^{2+} ions with high-spin configuration ($S = 3/2$) on octahedral sites are connected to form one-dimensional ferromagnetic zigzag chains along the c axis. In the ab plane, isosceles triangles are formed by Co^{2+} ions [17–21]. The intrachain ferromagnetic interaction (nearest neighbor) is 2.74 meV and the interchain antiferromagnetic interactions (next nearest neighbor) are about 0.4 meV, according to the INS experiment [7]. $CoNb_2O_6$ undergoes two successive magnetic phase transitions to incommensurate magnetic ordering at $T_{N1} = 2.9$ K and to antiferromagnetic ordering with magnetic propagation vector (0,0.5,0) at $T_{N2} = 1.9$ K. Below T_{N1}, Co^{2+} spins within a chain are aligned ferromagnetically. Because of the finite antiferromagnetic interactions along a and b axes, antiferromagnetic coupling works between chains. The magnetic easy axis of a Co^{2+} ion lies within the ac plane away by $\pm 31°$ from c axis [Fig. 1(a)]. The hard axis is parallel to the b axis. The TIM Hamiltonian for each chain in $CoNb_2O_6$ is expressed as

$$\hat{\mathcal{H}}_{\mathrm{TIM}} = -J_0 \sum_i S_i^z S_{i+1}^z - \Gamma \sum_i S_i^x, \tag{1}$$

where J_0 is the ferromagnetic exchange interaction between the nearest-neighboring Co sites along the chain ($J_0 > 0$). S_i^z and S_i^x are the easy- and hard-axis components of the spin at site i, Γ corresponds to the transverse magnetic field along the magnetic hard $b(\|x)$ axis.

In the present study, we investigate the elastic response induced by quantum fluctuations close to the QCP in $CoNb_2O_6$ by means of ultrasound technique. Measurements in magnetic field enable us to detect spin-orbit fluctuations coupled to strain. We observed a huge

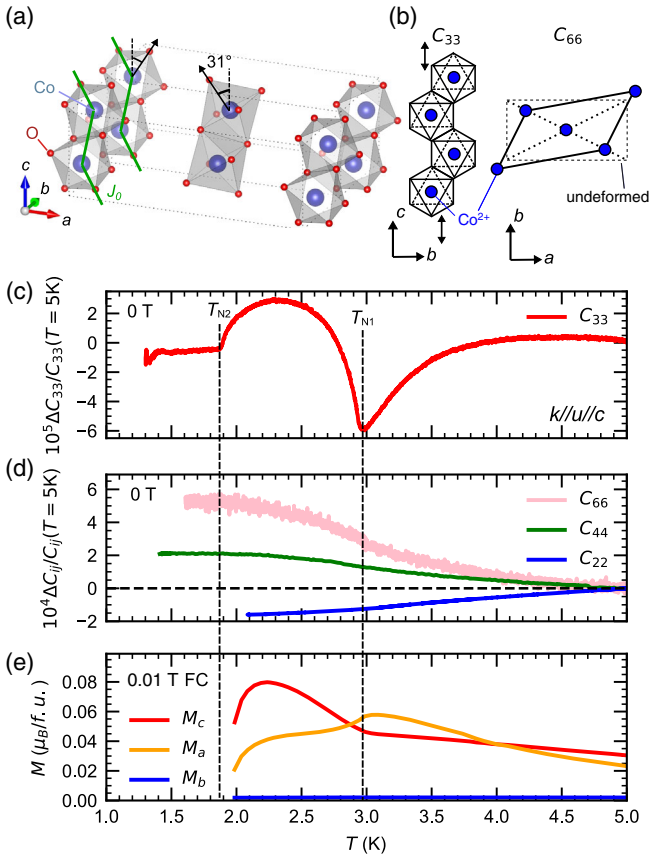

FIG. 1. (a) Crystal structure of $CoNb_2O_6$. Black arrows are the spin directions in the magnetically ordered phase. J_0 and H are the intrachain exchange interaction and transverse magnetic field, respectively. (b) Schematic illustration of the strain for the modes C_{33} and C_{66}. (c) Temperature dependence of the relative change of the elastic constant $\Delta C_{33}/C_{33}$ at 0 T, obtained by measuring the velocity of longitudinal ($\boldsymbol{k}\|\boldsymbol{u}$) ultrasound propagating along the c axis ($\boldsymbol{k}\|c$). (d) Temperature dependence of the relative change of the elastic constants C_{22} ($\boldsymbol{k}\|\boldsymbol{u}\|b$), C_{44} ($\boldsymbol{k}\|b, \boldsymbol{u}\|c$), and C_{66} ($\boldsymbol{k}\|b, \boldsymbol{u}\|a$). (e) Temperature dependence of the magnetization with a field of 0.01 T applied along the a, b, and c direction (M_a, M_b, and M_c) measured in field-cooled (FC) mode.

lattice softening of the C_{66} mode near the QCP when applying a transverse magnetic field. Our results indicate a critical softening of this mode due to quantum critical fluctuations.

Single crystals of $CoNb_2O_6$ were grown by the floating-zone method. Stoichiometric amounts of CoO and Nb_2O_5 were mixed and pressed into rods. The rods were heated at 1100 K for 24 h in air flow to obtain feed and seed rods. The feed rod was melted in air flow at a growth rate ~3.0 mm/h by using a floating zone furnace. The crystals were characterized by powder x-ray diffraction and magnetization measurements. The crystalline bar was cut into a cuboid shape with dimensions of approximately $3 \times 4 \times 3$ mm^3. For the ultrasound experiments, two parallel surfaces of (100), (010), or (001) in the orthorhombic setting were prepared. Piezoelectric polymer foils for longitudinal-wave and 41° X-cut $LiNbO_3$ transducers for transverse-wave excitations were glued to these surfaces for generating and detecting ultrasound waves. In the following, $\boldsymbol{k}$ and $\boldsymbol{u}$ represent propagation and polarization directions of ultrasound waves, respectively. The ultrasound frequencies were in the range of 10–130 MHz. By using a pulse-echo method with phase-comparison technique [22], the relative change $\Delta v/v$ of the sound velocity was measured as a function of temperature and magnetic field. For obtaining the elastic constant C_{ij}, we used the relation $C_{ij} = \rho v^2$, where ρ is the mass density. The relative change of the elastic constant was calculated as $\Delta C_{ij}/C_{ij} = 2(\Delta v/v) + (\Delta v/v)^2$.

Figures 1(c) and 1(d) show the temperature dependence of various elastic constants below 5 K at 0 T. The corresponding temperature dependences of the magnetization with field applied along the a, b, and c axes are displayed in Fig. 1(e). The elastic constant C_{33} decreases toward T_{N_1} and T_{N_2}, as shown in Fig. 1(c), although the magnitude of the relative change in C_{33} is within the order of some 10^{-3}%. In contrast, no distinct anomaly appears in the other elastic constants [Fig. 1(d)]. Obviously, only C_{33} is sensitive to the two magnetic phase transitions in $CoNb_2O_6$. Note, that no structural phase transition has been reported so far in this system at low temperatures [13,23]. The C_{33} mode modulates the distance between neighboring Co^{2+} ions in the chain [Fig. 1(b)], leading to a modulation of the dominant intrachain magnetic interaction J_0 due to exchange-striction coupling. The transverse acoustic modes, such as C_{66} or C_{44}, may contribute to the exchange-striction in case of the indirect magnetic exchange interaction, because they mainly modulate the angles [Fig. 1(b)] rather than the distances. Moreover, the anomaly size at T_{N1} for each (transverse or longitudinal) mode depends on the corresponding spin-strain coupling constants, which values are unknown.

The magnetic-field dependence of the elastic constant C_{66} was measured in the configuration $\boldsymbol{k}\|\boldsymbol{H}\|b$ and $\boldsymbol{u}\|a$ at various temperatures [Fig. 2(a)]. As a most important result, we observe a huge softening of C_{66} of about 20% at 4.8 T and 1.3 K. The softening in C_{66} in a transverse field is about 4 orders of magnitude larger than that of C_{33} at 0 T. With increasing temperature, the magnitude of the softening becomes smaller, the width of the dip structure in C_{66} becomes wider, and the dip position moves to lower field. The C_{66} anomaly almost disappears above 4.0 K. Obviously, the softening in C_{66} is related to the vicinity of the QCP. Approaching the QCP, the elastic minimum grows dramatically and the softening seems to become critical. This suggests that the fluctuating d_{xy} orbitals strongly couple to the u_{xy} strain related to the C_{66} mode. The modes C_{22} and C_{33}, measured at 1.3 K, are largely independent from the applied magnetic field [Fig. 2(b)]. Only C_{44} shows some broad field-dependent features with the more than 1% change indicating possible involvement

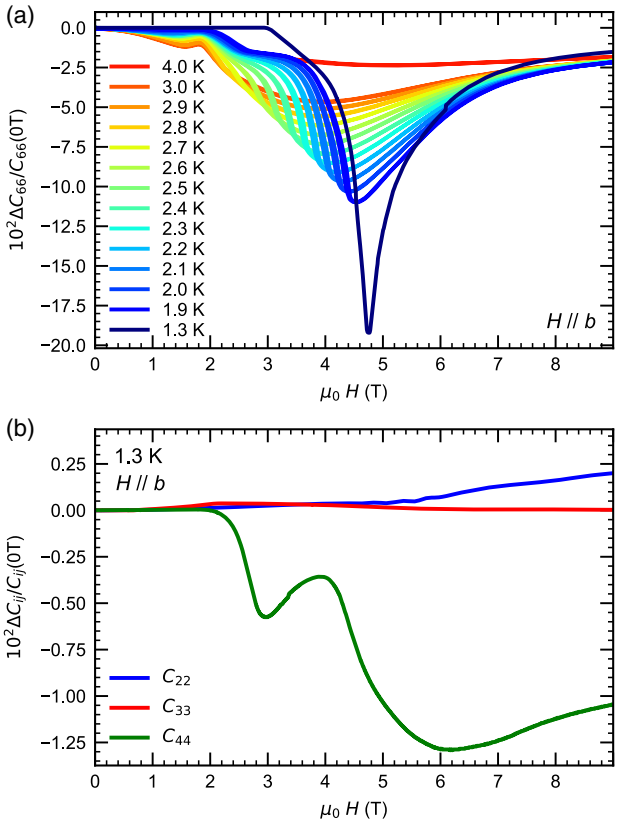

FIG. 2. (a) Magnetic-field dependence of the elastic constant C_{66} at various temperatures. For this transverse ultrasound wave propagates along b and the atoms oscillate along the a direction. (b) Magnetic-field dependence of the elastic constants C_{22}, C_{33}, and C_{44} at 1.3 K.

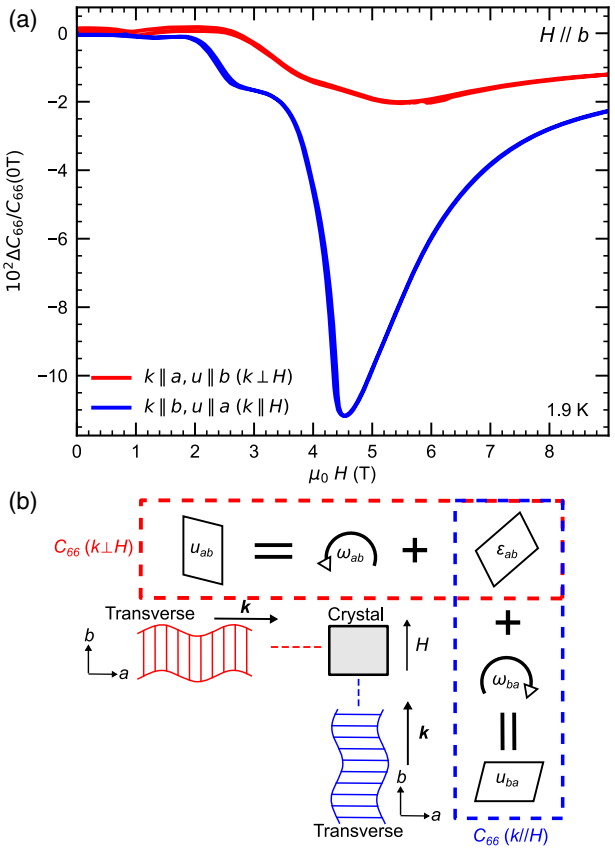

FIG. 3. (a) Magnetic-field dependence of the relative change of the elastic constant C_{66} obtained from the measurements of two C_{66} modes in the Faraday ($\boldsymbol{k}\|b\|\boldsymbol{H}$, $\boldsymbol{u}\|a$, blue line) and Voigt ($\boldsymbol{k}\|a$, $\boldsymbol{u}\|\boldsymbol{H}\|b$, red line) configurations at 1.9 K. (b) Schematic illustration of the rotational invariance effect.

of the d_{yz} orbitals and complexity of the quantum critical regime. However, since the change of the C_{66} mode is much larger than that of the C_{44} mode, the anomaly in the C_{66} mode is uniquely coupled to the quantum critical region (see also Supplemental Material [14]). Several anomalies observed in the low-field region are almost independent on the magnetic field and temperature, which indicates that these anomalies are not related to the quantum criticality [14]. Moreover, the huge anomaly in the applied magnetic field [Fig. 2(a)] and no substantial anomalies in zero magnetic field [Fig. 1(d)] indicate a significant enhancement of the spin-orbital-strain interaction close to the QCP.

In order to specify the origin of the anomaly in C_{66}, we performed measurements in two different geometries in more detail. In one geometry, the transverse-ultrasound mode oscillates along the a axis ($\boldsymbol{u}\|a$) and propagates along the b axis ($\boldsymbol{k}\|b$) parallel to the magnetic field $\boldsymbol{H}$ ($\boldsymbol{k}\|\boldsymbol{H}$, Faraday configuration). In the other geometry, ultrasound oscillating along the b axis propagates along the a axis ($\boldsymbol{k}\|a$) is perpendicular to the magnetic field H ($\boldsymbol{k}\perp\boldsymbol{H}$, Voigt configuration). As shown in Fig. 3(a), there is a minimum for both geometries, but the large softening is observed only in the Faraday configuration. The difference of relative change in C_{66} was about 10% at $T = 1.9$ K. The difference of the equivalent elastic constants between $\boldsymbol{k}\|\boldsymbol{H}$ and $\boldsymbol{k}\perp\boldsymbol{H}$ configurations is due to the rotational invariance effect (RIE) [22]. A schematic illustration of the RIE is presented in Fig. 3(b). The induced deformation by a transverse ultrasound wave $u_{ij} = \partial u_i/\partial x_j$ is given by the sum of the symmetric tensor $\epsilon_{ij} = 1/2(\partial u_i/\partial x_j + \partial u_j/\partial x_i)$ and the antisymmetric tensor $\omega_{ij} = 1/2(\partial u_i/\partial x_j - \partial u_j/\partial x_i)$, where x_i denotes variational directions. Thus, the induced deformation is $u_{ab} = \epsilon_{ab} + \omega_{ab}$ for the Voigt and $u_{ba} = \epsilon_{ab} - \omega_{ab}$ for the Faraday configuration, where $\omega_{ba} = -\omega_{ab}$. Both configurations induce the same symmetric strain ϵ_{ab} in C_{66}, which should cause no difference between these two geometries without magnetic effects. The interaction between the quadrupole moments and the lattice rotation causes the difference between the Faraday and Voigt modes. Although elastic softenings have been observed and understood in terms of quadrupolar interactions [24–27], only small RIEs of typically 0.5% were reported in f-electron systems [22], such as $HoVO_4$ [28], $CeAl_2$ [29], and TmSb [30]. The RIE of about 10% at 1.9 K in $CoNb_2O_6$ is extremely large.

Let us consider the electronic states of Co^{2+} in a CoO_6 octahedron cluster. The ground state can be represented by the linear combinations of the lowest-energy triplet states. Value of the SOI constant λ in a free Co^{2+} ion is 22 meV [16]. Considering the perturbation of the triplet states from SOI, the wave functions of the lowest-lying doublet are represented by $j_{\mathrm{eff}} = \pm 1/2$ [16,31–33]. In fact, in $CoNb_2O_6$ the local-site symmetry of the Co^{2+} ion is lowered to C_2 symmetry and, thus, the SOI might be comparable to the crystal-field splitting [34]. Thus, the actual wave functions in the ground state might be complex but the spin and orbital degrees of freedom should be coupled. Using the simple CoO_6 cluster model, we can show that SOI plays an essential role in the induction of RIE [14]. Thus, spin fluctuations can couple to orbital fluctuations via SOI, which might explain the RIE enhancement near the QCP.

Finally, we discuss the temperature dependence of C_{66} ($\boldsymbol{k}\|\boldsymbol{H}$) in constant magnetic fields [Fig. 4(a)]. In 2 T, C_{66} shows a clear minimum at 3 K indicating 3D magnetic ordering. At 4 T, the minimum appears at about 2 K, whereas at 5 T and above, a strong lattice softening, but no minimum is visible down to 1.5 K. Considering the strong softening, it is plausible to assume a bilinear coupling of the ϵ_{xy} strain (C_{66} mode) with the d_{xy} electron orbitals. In this case, we can describe the temperature dependence of the elastic constant by using the Curie-Weiss-type equation [22], which includes the coupling of microscopic strain to the orbital and orbital-orbital interactions.

$$C(T) = C^{(0)}\left(\frac{T - T_C^0}{T - \Theta}\right), \tag{2}$$

where $C^{(0)}$ is the background elastic constant independent of spin and orbital. Θ represents the correlation between orbitals, which corresponds to the Weiss temperature in the magnetic susceptibility. T_C^0 is the sum of Θ and the Jahn-Teller energy E_{JT}, that is, $T_C^0 = \Theta + E_{\mathrm{JT}}$. E_{JT} represents the interaction between the strain and orbital at a single site. The temperature dependences are well described by the Curie-Weiss law. Obviously, the magnetic ordering prevents further development of orbital fluctuations [Fig. 4(a)]. The fits provide further insight to the orbital states. The magnetic-field dependence of fit parameters are shown in Fig. 4(b). E_{JT} has a small value and changes only by about 0.1 K as a function of the applied magnetic field, which indicates that the single-ion strain-orbital coupling is not responsible for the large softening. In contrast, Θ changes from 2 K at 2 T to −3 K at 8 T. Remarkably, our simplified approach suggests that the sign of Θ changes from positive to negative, which reflects the change of orbital correlations from ferroic to antiferroic in the vicinity of the QCP. In other words, the orbital correlations seem to dominate the quantum critical behavior. At this stage, we cannot exclude other possible phenomena such as magnetic field assisted orbital quenching and orbital reordering due to orbital correlations, or higher-order multipolar ordering. A more elaborated theory would be of interest to further address this issue.

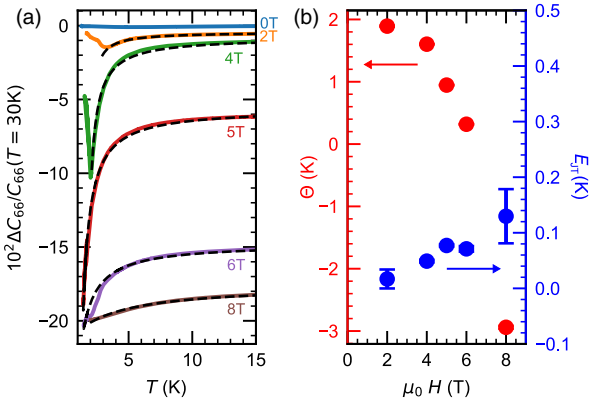

FIG. 4. (a) Temperature dependence of the relative change of the elastic constant C_{66} ($\boldsymbol{k}\|\boldsymbol{H}$) in various applied magnetic fields. The black dashed lines are Curie-Weiss fits (see main text). We shifted each curve for better visibility. (b) Magnetic-field dependence of the parameters (Θ and E_{JT}) from the Curie-Weiss fits.

In conclusion, we observed a huge softening of the elastic constant C_{66} in $CoNb_2O_6$ approaching the QCP when applying a transverse magnetic field. The anomaly in C_{66} is assumed to originate from spin-orbit-strain-coupled fluctuations. Moreover, we observed anisotropic elastic responses for two crystallographically equivalent C_{66} modes exhibiting the RIE in the vicinity of the QCP. Both the strong softening of the C_{66} mode and large RIE confirm a crucial role of the quadrupolar degrees of freedom in the quantum critical regime of this transverse Ising magnet. We propose that the critical softening originates from SOI and is largely enhanced by the quantum fluctuations at the QCP. The RIE has been intensively studied in the field of spintronics in terms of the mechanical generation of spin current [35]. We believe that the understanding of the relationship between quantum criticality and RIE should be also important for the spintronics.

We acknowledge support from the DFG through the Würzburg-Dresden Cluster of Excellence on Complexity and Topology in Quantum Matter *ct.qmat* (EXC 2147, Project No. 39085490) and by the Dresden High Magnetic Field Laboratory (HLD) at HZDR, member of the European Magnetic Field Laboratory (EMFL). High-energy Laue photographs, magnetization and other ultrasound measurements were carried out at the Institute for Solid State Physics (ISSP), the University of Tokyo. We are grateful to S. Mombetsu, H. Mitamura, N. D. Khanh, Y. Fujima, and T. Sato for helpful comments. K. M. is supported by the Japan Society for the Promotion of

Science through the Program for Leading Graduate Schools (Materials Education program for the future leaders in Research, Industry, and Technology (MERIT)) and a JSPS Research Fellowship for Young Scientists (JSPS KAKENHI Grant No. JP15J08412). This research was also supported by the MERIT Overseas Dispatch program. The crystal structures are visualized by using VESTA 3 [36].

*Present address: RIKEN Center for Emergent Matter Science, Wako 351-0198, Japan.
keisuke.matsuura@riken.jp

[1] G. R. Stewart, Rev. Mod. Phys. **73**, 797 (2001).
[2] M. Vojta, Rep. Prog. Phys. **66**, 2069 (2003).
[3] H. v. Löhneysen, A. Rosch, M. Vojta, and P. Wölfle, Rev. Mod. Phys. **79**, 1015 (2007).
[4] S. Sachdev and B. Keimer, Phys. Today **64**, No. **2**, 29 (2011).
[5] T. Shibauchi, A. Carrington, and Y. Matsuda, Annu. Rev. Condens. Matter Phys. **5**, 113 (2014).
[6] S. Sachdev, *Quantum Phase Transitions* (Cambridge University Press, Cambridge, England, 1999).
[7] R. Coldea, D. A. Tennant, E. M. Wheeler, E. Wawrzynska, D. Prabhakaran, M. Telling, K. Habicht, P. Smeibidl, and K. Kiefer, Science **327**, 177 (2010).
[8] P. Pfeuty, Ann. Phys. (N.Y.) **57**, 79 (1970).
[9] D. Bitko, T. F. Rosenbaum, and G. Aeppli, Phys. Rev. Lett. **77**, 940 (1996).
[10] Z. Wang, T. Lorenz, D. I. Gorbunov, P. T. Cong, Y. Kohama, S. Niesen, O. Breunig, J. Engelmayer, A. Herman, J. Wu, K. Kindo, J. Wosnitza, S. Zherlitsyn, and A. Loidl, Phys. Rev. Lett. **120**, 207205 (2018).
[11] C. M. Morris, R. Valdés Aguilar, A. Ghosh, S. M. Koohpayeh, J. Krizan, R. J. Cava, O. Tchernyshyov, T. M. McQueen, and N. P. Armitage, Phys. Rev. Lett. **112**, 137403 (2014).
[12] A. W. Kinross, M. Fu, T. J. Munsie, H. A. Dabkowska, G. M. Luke, S. Sachdev, and T. Imai, Phys. Rev. X **4**, 031008 (2014).
[13] T. Liang, S. M. Koohpayeh, J. W. Krizan, T. M. McQueen, R. J. Cava, and N. P. Ong, Nat. Commun. **6**, 7611 (2015).
[14] See Supplemental Material at http://link.aps.org/supplemental/10.1103/PhysRevLett.124.127205 for details about the calculation.
[15] W. J. L. Buyers, T. M. Holden, E. C. Svensson, R. A. Cowley, and M. T. Hutchings, J. Phys. C **4**, 2139 (1971).
[16] K. Tomiyasu, M. K. Crawford, D. T. Adroja, P. Manuel, A. Tominaga, S. Hara, H. Sato, T. Watanabe, S. I. Ikeda, J. W. Lynn, K. Iwasa, and K. Yamada, Phys. Rev. B **84**, 054405 (2011).
[17] T. Hanawa, K. Shinkawa, M. Ishikawa, K. Miyatani, K. Saito, and K. Kohn, J. Phys. Soc. Jpn. **63**, 2706 (1994).
[18] C. Heid, H. Weitzel, P. Burlet, M. Bonnet, W. Gonschorek, T. Vogt, J. Norwig, and H. Fuess, J. Magn. Magn. Mater. **151**, 123 (1995).
[19] S. Kobayashi, S. Mitsuda, and K. Prokes, Phys. Rev. B **63**, 024415 (2000).
[20] H. Weitzel, H. Ehrenberg, C. Heid, H. Fuess, and P. Burlet, Phys. Rev. B **62**, 12146 (2000).
[21] S. Lee, R. K. Kaul, and L. Balents, Nat. Phys. **6**, 702 (2010).
[22] B. Lüthi, *Physical Acoustics in the Solid State* (Springer, New York, 2005).
[23] E. M. Wheeler, Ph.D. thesis, Clarendon Laboratory, Department of Physics, Oxford University, 2007.
[24] T. Suzuki, I. Ishii, N. Okuda, K. Katoh, T. Takabatake, T. Fujita, and A. Tamaki, Phys. Rev. B **62**, 49 (2000).
[25] T. Watanabe, S. Yamada, R. Koborinai, and T. Katsufuji, Phys. Rev. B **96**, 014422 (2017).
[26] S. Kamikawa, I. Ishii, K. Takezawa, T. Mizuno, T. Sakami, F. Nakagawa, H. Tanida, M. Sera, T. Suzuki, K. Mitsumoto, and X. Xi, Phys. Rev. B **96**, 155131 (2017).
[27] I. Ishii, X. Xi, Y. Noguchi, T. Mizuno, S. Kumano, K. Araki, K. Katoh, and T. Suzuki, AIP Adv. **8**, 101315 (2018).
[28] T. Goto, A. Tamaki, T. Fujimura, and H. Unoki, J. Phys. Soc. Jpn. **55**, 1613 (1986).
[29] B. Lüthi and C. Lingner, Z. Phys. B **34**, 157 (1979).
[30] P. S. Wang and B. Lüthi, Phys. Rev. B **15**, 2718 (1977).
[31] M. E. Lines, Phys. Rev. **131**, 546 (1963).
[32] J. P. Goff, D. A. Tennant, and S. E. Nagler, Phys. Rev. B **52**, 15992 (1995).
[33] T. Nguyen, S. E. Nagler, R. A. Cowley, T. Perring, and R. Osborn, J. Phys. Condens. Matter **7**, 2917 (1995).
[34] R. Borromei, E. Cavalli, and G. Ingletto, Phys. Status Solidi B **117**, 733 (1983).
[35] M. Matsuo, J. Ieda, E. Saitoh, and S. Maekawa, Phys. Rev. Lett. **106**, 076601 (2011).
[36] K. Momma and F. Izumi, J. Appl. Crystallogr. **44**, 1272 (2011).